Original paper

Supergene uranyl molybdates (calcurmolite, iriginite and umohoite) from the Majerská valley U–Mo occurrence near Čučma, Slovakia: Mineralogy, chemical composition and Raman spectroscopy

Martin ŠTEVKO[1,2*], Jiří SEJKORA[2], Štefan FERENC[3]

[1] *Earth Science Institute v.v.i., Slovak Academy of Sciences, Dúbravská cesta 9, 840 05 Bratislava, Slovakia; martin.stevko@savba.sk*
[2] *Department of Mineralogy and Petrology, National Museum, Cirkusová 1740, 193 00 Prague 9, Czech Republic*
[3] *Department of Geography and Geology, Faculty of Natural Sciences, Matej Bel University, Tajovského 40, 974 01 Banská Bystrica, Slovakia*
[*] *Corresponding author*

A new occurrence of three rare supergene uranyl molybdates, calcurmolite, iriginite and umohoite was recently discovered at the Majerská valley U–Mo prospect near Čučma, Spišsko-gemerské rudohorie Mts., Slovakia. Calcurmolite is the most common uranyl molybdate at the studied locality, followed by relatively common iriginite and rare umohoite. In this paper, we present their detailed mineralogical study, including paragenetic observations, X-ray powder diffraction, chemical composition, and a Raman spectroscopic study. The quantitative chemical (WDS) data indicate a significant presence of Fe (around 0.35 apfu) in both iriginite and umohoite, whereas Na and K are typical minor elements observed in calcurmolite. The studied assemblage of supergene uranyl molybdates was formed by in-situ weathering of uraninite–molybdenite aggregates under the relatively acidic conditions, caused by breakdown of abundant pyrite and absence of carbonates.

Keywords: uranyl molybdates, calcurmolite, iriginite, umohoite, chemical composition, Raman spectroscopy
Received: 29 October 2025; accepted: 4 December 2025; handling editor: J. Plášil
We dedicate this paper to the memory of Ing. Jiří Čejka, DrSc. (1929–2025), a prominent Czech mineralogist and chemist who specialized in the study of uranium minerals.

1. Introduction

Natural uranyl molybdates represent a small group of relatively rare supergene minerals that form under the oxidizing, mostly acidic conditions at various genetic types of U–Mo deposits (Finch and Murakami 1999; Krivovichev and Plášil 2013; Kuporev et al. 2024). Only nine uranyl molybdates are known in nature, including umohoite (Brophy and Kerr 1953), calcurmolite (Rudnitskaya 1959), moluranite and iriginite (Epshtein 1959), mourite (Kopchenova et al. 1962), sedovite (Skvortsova and Sidorenko 1965), tengchongite (Chen et al. 1986), deloryite (Sarp and Chiappero 1992) and baumoite (Elliot et al. 2019), of which umohoite and iriginite are the most common ones (Krivovichev and Plášil 2013). On the other hand, a large group of synthetic molybdates of uranyl containing various cations such as Ag, K, Na, Cs, Rb, Li, Ca or Tl was described (e.g., Krivovichev and Burns 2000a, b, 2001a, b, 2002a, b, c, d, 2003a, b; Obbade et al. 2003; Nazarchuk et al. 2005a, b; Alekseev et al. 2007; Kuporev et al. 2024; Nazarchuk et al. 2025). Detailed knowledge of chemical composition, crystal-chemistry, and stability of uranyl molybdates is essential for understanding the processes leading to *in-situ* or post-mining weathering of natural uranium minerals, mobility of uranium, as well as alteration of spent nuclear waste (Buck et al. 1997; Burns 1999; Finch and Murakami 1999).

Calcurmolite is a rare calcium uranyl molybdate, which is known only from a small number of localities, especially U–Mo deposits in Armenia (Rudnitskaya 1959; Sidorenko et al. 2005; Frost et al. 2008) and Kazachstan (Fedorov 1963; Skvortsova et al. 1969; Sidorenko et al. 2005). It was also described from the uranium deposits in Yunnan province in China (Chen et al. 1986, 1990), Rabejac U deposit in France (Deliens 1992; Dal Bo 2018) and Paulding uranium prospect in Michigan, USA (Robinson and Carlson 2013). Calcurmolite was long considered as monoclinic phase (e.g., Sidorenko et al. 2005; Dal Bo et al. 2018), but a recent single-crystal precession electron-diffraction tomography study of calcurmolite from Rabejac (Steciuk et al. 2020) confirmed its triclinic symmetry. Iriginite and umohoite are the most common minerals among natural uranyl molybdates, described from several U–Mo or U deposits in Kazakhstan (Skvortsova et al. 1961; Sidorenko et al. 2003), Russia (Epshtein 1959; Chernikov et al. 1997), Germany (Grö-

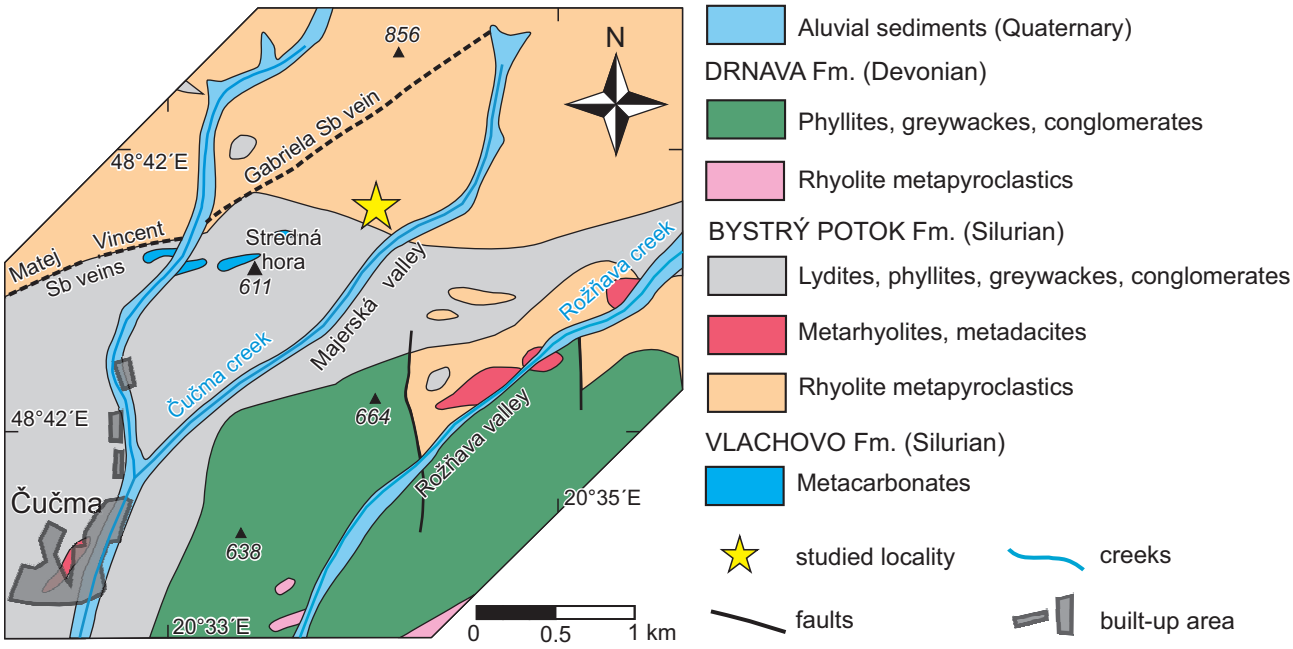

Fig. 1 Regional geological setting of the Majerská dolina U–Mo occurrence (modified after Bajaník et al. 1984).

bner and Kolitsch 2007), France (Dal Bo et al. 2018), Czech Republic (Pauliš et al. 2019), DR Kongo (Deliens 1975; Piret and Deliens 1976, 1977) or USA (e.g., Brophy and Kerr 1953; Coleman and Appleman 1957; Hamilton and Kerr 1959; Stephenson 1964). Crystal structures of both iriginite and umohoite were most recently revised by Krivovichev and Burns (2000a, b).

A new occurrence of three uranyl molybdates, calcurmolite, iriginite and umohoite was recently discovered at the Majerská valley U–Mo prospect near Čučma, Slovakia. Here we report results of their detailed mineralogical study, including paragenetic observations, chemical composition and Raman spectroscopy.

2. Localization and geological setting

The occurrence of hydrothermal U–Mo mineralization with supergene uranyl molybdates is situated in the Majerská valley, around 3.5 km NE of the Čučma village, 6.3 km NNE of the Rožňava town in the Spišsko-gemerské rudohorie Mts., Rožňava Co., Košice Region, Slovakia. The studied samples with uranyl molybdates were collected by M. Števko in May 2020 in the exploration trench Ča–13. GPS coordinates of the studied site (exploration trench Ča–13) are 48.714240° N, 20.567221° E, 608 m a.s.l.

The two principal types of hydrothermal uranium mineralization were distinguished at the Majerská valley area: 1) quartz–fluorapatite veins with REE phosphates, uraninite and only minor sulfides or 2) quartz veins with only minor fluorapatite and U–Mo mineralization represented by abundant uraninite, molybdenite and numerous other sulfides, sulfosalts and tellurides (Ferenc et al. 2019, 2021). Hydrothermal U–Mo mineralization at the Majerská valley occurrence is represented by three short, lenticular quartz veins hosted in the acidic metapyroclastic rocks of the Early Paleozoic (Silurian) Bystrý Potok Formation (Fig. 1), belonging to the Gelnica Group and the Gemeric tectonic unit. The veins are up to 0.3 m thick, they are arranged in accordance with the metamorphic foliation of the surrounding rocks, have a direction of 65–67° to the NE and dip of about 36° to the SE (Šváb et al. 1966, Donát 1998). All tree veins were exposed by the exploration trench Ča–13 (Fig. 2), which was excavated in 1960s during the exploration for

Fig. 2 Remains of the exploration trench Ča–13 at the Majerská valley U–Mo occurrence. Situation in May 2020.

uranium ores (Šváb et al. 1966) and later re-excavated in 1990s (Donát 1998).

Mineralogy of the hydrothermal quartz veins with U–Mo mineralization in the Majerská valley area was recently studied in detail by Ferenc et al. (2019, 2021). Quartz is the principal gangue mineral accompanied by only accessory fluorapatite, zircon, schorl-dravite, rutile, Fe–Ti and U–Ti oxides, muscovite, chlorite, and titanite. The most abundant ore minerals are molybdenite and uraninite, accompanied by a diverse assemblage of sulfides (pyrite, minor galena), sulfoarsenides (cobaltite, gersdorffite, ullmannite), sulfosalts (bismuthinite, minerals of the kobellite–tintinaite series, cosalite, jamesonite), sulfotellurides (tetradymite, joséite-A, joséite-B), ikunolite and native bismuth. Ore minerals are distributed in quartz very irregularly in the form of fine-grained bands and nests. Supergene minerals are represented by bassetite, saléeite, autunite, torbernite, zeunerite, phosphuranylite, wulfenite, and other poorly identified Pb–Bi–Sb–Mo oxides. Ferenc et al. (2019) also reported the presence of uranyl molybdate, iriginite at the Majerská valley occurrence. Števko (2022) later briefly described the assemblage of three uranyl molybdates (calcurmolite, iriginite, and umohoite) from this locality. The chemical *in-situ* electron-microprobe U–Pb dating of uraninite from the Majerská valley U–Mo occurrence yielded an average age around 265 Ma and thus confirmed the direct connection of the hydrothermal U–Mo mineralization with the intrusions of post-collisional Gemeric S-type granites (Ferenc et al. 2019).

3. Analytical methods

A detailed study of morphology and paragenetic relations of uranyl molybdates was carried out on uncoated samples in low-vacuum mode on a Hitachi S3700-N scanning electron microscope (Department of Paleontology, National Museum, Prague, Czech Republic).

Quantitative chemical analyses of uranyl molybdates were performed using a Cameca SX100 electron microprobe (Department of Mineralogy and Petrology, National Museum, Prague, Czech Republic) operating in WDS mode (accelerating voltage 15 kV, probe current 4 nA, 3–20 μm beam width). The following standards and X-ray lines were used: albite (Na*K*α), apatite (Ca*K*α, P*K*α), baryte (Ba*L*α), celestine (S*K*α, Sr*L*β), chalcopyrite (Cu*K*α), clinoclase (As*L*α), Co (Co*K*α), Cr_2O_3 (Cr*K*α), diopside (Mg*K*α), halite (Cl*K*α), hematite (Fe*K*α), LiF (F*K*α), Ni (Ni*K*α), rhodonite (Mn*K*α), sanidine (Al*K*α, Si*K*α, K*K*α), TiO_2 (Ti*K*α), UO_2 (U*M*α), vanadinite (V*K*α), wulfenite (Pb*M*α, Mo*L*α), YVO_4 (Y*L*α) and ZnO (Zn*K*α). Contents of the above-listed elements, which are not included in the table, were analysed quantitatively, but their concentrations were consistently below the detection limit (ca. 0.03–0.05 wt. % for individual elements). Raw intensities were converted to the concentrations of elements using the automatic "PAP" matrix-correction algorithm (Pouchou and Pichoir 1985).

Powder X-ray diffraction data of calcurmolite and iriginite were recorded at room temperature using a Bruker D8 Advance diffractometer (Department of Mineralogy and Petrology, National Museum, Prague, Czech Republic) equipped with a solid-state LynxEye detector and secondary monochromator producing Cu*K*α radiation operating at 40 kV and 40 mA (Bragg-Brentano geometry, 4–70° 2θ, step 0.01° and counting time of 10 s per step). Positions and intensities of reflections were found and refined using the PearsonVII profile-shape function with the ZDS program package (Ondruš 1993), and the unit-cell parameters were refined by the least-squares algorithm implemented by Burnham (1962). The experimental powder patterns were indexed in line with the calculated values of intensities obtained from the crystal structure of calcurmolite (Steciuk et al. 2020) and iriginite (Krivovichev and Burns 2002b), based on PowderCell2.3 program (Kraus and Nolze 1996).

The Raman spectra of uranyl molybdates were collected in the range 4000–60 cm^{-1} using a DXR dispersive Raman Spectrometer (Thermo Scientific) mounted on a confocal Olympus microscope (Department of Mineralogy and Petrology, National Museum, Prague, Czech Republic). The Raman signal was excited by an unpolarised red 633 nm He–Ne gas laser and detected by a CCD detector. The experimental parameters were: 100 × objective, 10 s exposure time, 300 exposures, 50 μm pinhole (calcurmolite and umohoite) or 50 μm slit (iriginite) spectrograph apertures and 8 mW (calcurmolite), 5 mW (iriginite), or 1 mW (umohoite) laser power levels. The spectra were repeatedly acquired from different grains to obtain a representative spectrum with the best signal-to-noise ratio. The eventual thermal damage of the measured point was excluded by visual inspection of the excited surface after measurement, by observation of possible decay of spectral features at the start of excitation and by checking for thermal downshift of Raman lines. The instrument was set up by a software-controlled calibration procedure using multiple neon emission lines (wavelength calibration), multiple polystyrene Raman bands (laser-frequency calibration) and standardized white-light sources (intensity calibration). Spectral manipulations were performed using the Omnic 9 software (Thermo Scientific). Tentative assignments of experimental spectra are based on papers of Čejka (1999), Nakamoto (2009) for H_2O, OH and UO_2^{2+} vibrations and Lunk et al. (2010), Moura et al. (2018), Vargas-Consuelos et al. (2023) for vibrations of the Mo octahedra. An empirical relation between energy of vibration and the corresponding bond

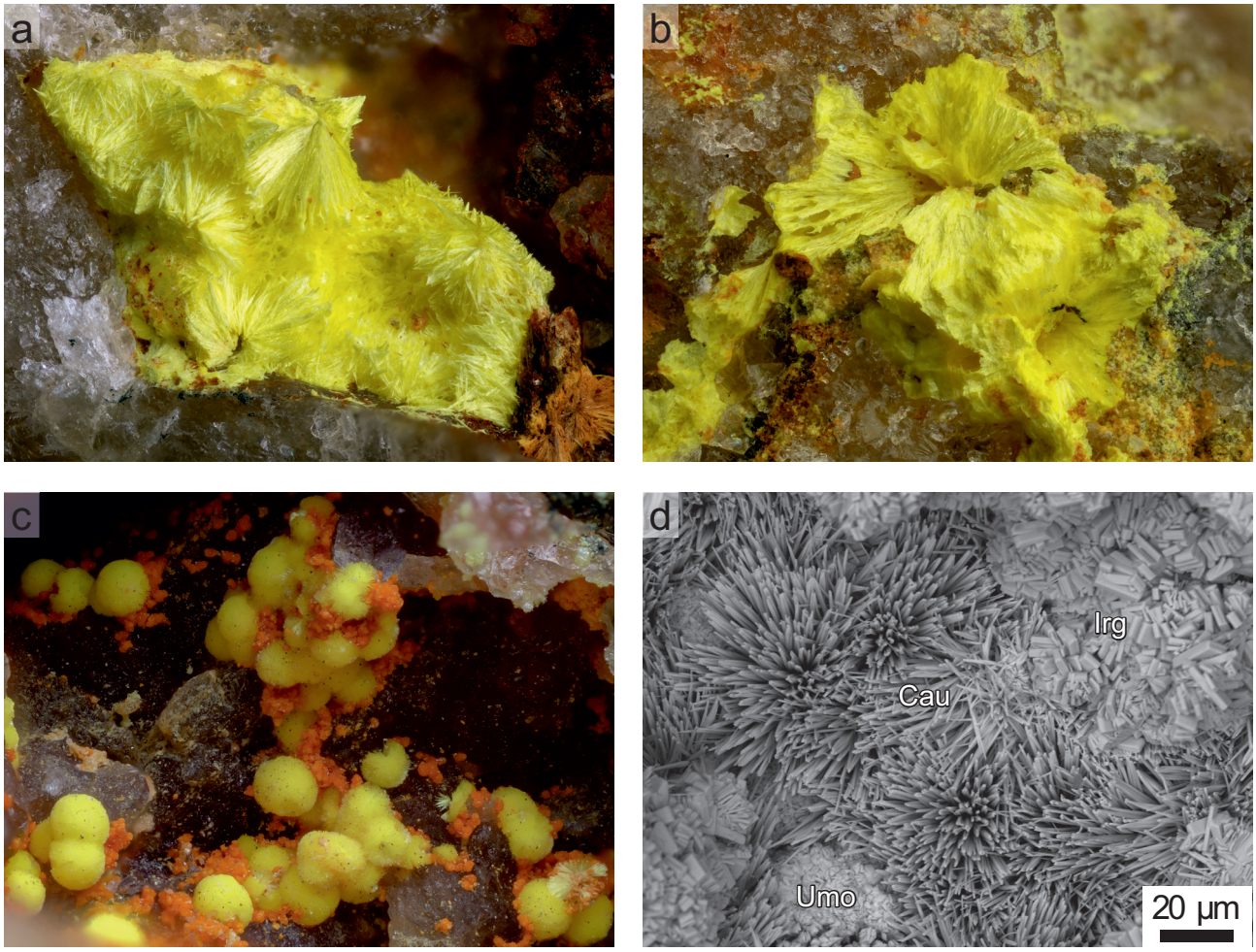

Fig. 3 Calcurmolite appearance: **a** – Radial aggregates of bright yellow calcurmolite consisting of individual acicular crystals. Field of view is 3 mm, photo L. Hrdlovič; **b** – Compact radial aggregates of calcurmolite. Field of view is 4 mm, photo L. Hrdlovič; **c** – Bright yellow spherical aggregates of calcurmolite partly overgrown by younger bright orange umohoite. Field of view is 3 mm, photo L. Hrdlovič; **d** – Radial groups of calcurmolite (Cau) overgrown by younger tabular crystals of iriginite (Irg). Minor umohoite (Umo) is also associated. BSE photo L. Váchová.

length (Libowitzky 1999) was used for the calculation of the O–H···O hydrogen-bond length. Another empirical relation given by Bartlett and Cooney (1989) was used for calculations of U–O bond lengths from wavenumbers of ν_3 and ν_1 UO_2^{2+} stretching vibrations.

4. Results

4.1. Calcurmolite

Calcurmolite is the most common uranyl molybdate at the studied locality. It forms bright yellow, radial to spherical aggregates up to 3 mm or microcrystalline coatings (Figs. 3a–d), which consist of individual, thin acicular crystals up to up to 500 µm long. Calcurmolite, as well as iriginite and umohoite, are most often found in small cavities or fractures in quartz, always in close proximity to weathered molybdenite-uraninite-pyrite aggregates. It is important to note that uranyl molybdates are present only if pyrite is strongly weathered or totally replaced by Fe oxides. Calcium, necessary for the formation of calcurmolite, was most probably liberated from accessory fluorapatite, as carbonates are absent. This idea is also supported by relatively abundant presence of phosphorus-dominant members of the autunite group (e.g., autunite, bassetite, saléeite, or torbernite) in the distant areas of quartz veins at the studied locality. Based on detailed paragenetic observations, calcurmolite is clearly older than associated iriginite (Fig. 3d). Its relationship with rare umohoite is more complex. In most of the cases, umohoite seems to be slightly younger than calcurmolite (Fig. 3c), but in one case, calcurmolite aggregates were also growing on umohoite. No supergene minerals other than Fe oxides (mixture of nanocrystalline ferrihydrite and goethite) were observed in direct association with uranyl molybdates.

The experimental powder X-ray diffraction pattern of calcurmolite (Tab. 1) shows a lot of similarities with data

published for calcurmolite from Kazakhstan and Armenia (Sidorenko et al. 2005) and agrees very well with a few diffraction maxima given for the sample from Rabejac by Steciuk et al. (2020). However, the data published by Deliens (1992) already shows more significant differences, but the comparison is complicated by the usual poorly crystalline nature of the samples. The refined unit-cell parameters of studied calcurmolite (triclinic space group *P*1, *a* 20.10(5), *b* 11.004(16), *c* 14.330(8) Å, α 84.81, β 112.74, γ 133.21(8)° and *V* 2057(11) Å^3) are comparable with data published by Steciuk et al. (2020) for sample from Rabejac deposit, Lodève basin, France obtained at 100K: *a* 19.6875, *b* 11.26, *c* 14.195 Å, α 84.4, β 112.5, γ 133.95° and *V* 2025 Å^3.

The chemical composition of the studied calcurmolite (Tab. 2) is generally close to the ideal formula $Ca[(UO_2)_3(MoO_4)_2(OH)_4](H_2O)_{\sim 5.0}$ recently proposed by Steciuk et al. (2020) based on crystal-chemical study of calcurmolite from Rabejac in France. In addition to the dominant presence of Ca (0.69–0.75 *apfu*), U (3 *apfu*) and Mo (1.99–2.13 *apfu*), the elevated contents of Na (up to 0.17 *apfu*), K (up to 0.21 *apfu*) and S (up to 0.09 *apfu*) as well as minor amounts of P (up to 0.01 *apfu*) and Cl (up to 0.04 *apfu*) were detected in the studied sample. Similar contents of Na were also reported in calcurmolite from Armenia and Kazakhstan (Skvortsova et al. 1969; Sidorenko et al. 2005) and elevated amounts of Na, K, S and P were observed in calcurmolite samples from France (Dal Bo et al. 2018; Steciuk et al. 2020). The average ($n = 11$) empirical formula of calcurmolite form the Majerská valley occurrence calculated on the basis of U = 3 *apfu* is $(Ca_{0.72}K_{0.15}Na_{0.03})_{\Sigma 0.90}(UO_2)_3(MoO_4)_{2.07}(SO_4)_{0.06}(PO_4)_{0.01}(OH)_{3.31}Cl_{0.03}\cdot 5H_2O$.

The full-range Raman spectrum of the studied calcurmolite is given in Fig. 4a; it is close to the spectrum of calcurmolite from the Gornoe U deposit, Transbaikal region, Russia (Fig. 4b) (R070028 of the RRUFF database, Lafuente et al. 2015) and is similar to published spectrum of calcurmolite from Sokh-Karasu area, Armenia (Frost et al. 2008). Bands of the very low intensity, located at 3477, 3245 and 2905 cm^{-1} (Fig. 4a), are connected with the ν OH stretching vibrations of hydrogen-bonded water molecules and hydroxyl groups, calculated O–H···O hydrogen-bond lengths

Tab. 1 Powder X-ray diffraction data of calcurmolite from the Majerská valley occurrence.

$d_{obs.}$	$I_{obs.}$	$d_{calc.}$	h	k	l
9.136	2.6	9.095	2	–1	0
7.744	100.0	7.746	0	1	0
6.385	1.9	6.382	0	0	2
5.976	2.8	5.971	0	1	1
5.713	1.8	5.704	0	–1	2
4.408	0.9	4.398	0	1	2
4.259	2.1	4.255	0	0	3
4.010	4.7	4.006	0	–2	1
		3.991	–5	2	1
3.874	12.9	3.873	0	2	0
3.557	3.9	3.550	–5	2	3
3.471	1.8	3.464	–5	1	3
3.344	4.2	3.340	2	–3	0
3.323	2.8	3.325	0	–2	3
3.262	4.6	3.263	0	–1	4
3.243	5.5	3.239	5	–2	1
3.190	13.8	3.191	0	0	4
2.851	2.3	2.852	0	–2	4
2.714	1.1	2.713	0	1	4
2.672	1.2	2.669	0	–3	1
2.583	0.7	2.582	0	3	0
2.552	0.6	2.553	0	0	5
2.4085	0.7	2.4121	0	3	1
2.2006	0.8	2.1990	0	2	4
1.9962	1.0	1.9954	–10	4	2
1.9891	0.6	1.9904	0	3	3
1.9749	0.5	1.9747	2	–2	6
1.9642	1.4	1.9649	0	–4	3
		1.9621	–10	4	4
1.5954	1.3	1.5955	0	0	8

Tab. 2 Quantitative chemical analyses of calcurmolite from the Majerská valley occurrence (in wt. %) and the calculated empirical formulae (*apfu*).

	mean	1	2	3	4	5	6	7	8	9	10	11
Na_2O	0.07	0.18	0.00	0.00	0.00	0.00	0.00	0.00	0.24	0.00	0.00	0.37
K_2O	0.52	0.45	0.49	0.39	0.52	0.50	0.46	0.53	0.51	0.49	0.74	0.63
CaO	2.99	3.13	3.37	2.95	3.06	2.90	2.88	3.02	2.98	2.79	2.92	2.92
P_2O_5	0.03	0.00	0.02	0.00	0.07	0.02	0.00	0.08	0.05	0.02	0.00	0.06
MoO_3	22.10	22.88	24.68	22.10	21.13	22.85	21.89	22.68	21.81	20.61	21.98	20.45
SO_3	0.37	0.39	0.34	0.20	0.46	0.34	0.40	0.41	0.26	0.46	0.27	0.51
UO_3	63.53	64.12	68.98	64.36	62.87	63.86	62.07	66.33	63.51	58.59	62.84	61.28
Cl	0.07	0.06	0.06	0.06	0.07	0.07	0.11	0.09	0.06	0.00	0.08	0.09
H_2O*	8.88	8.95	9.57	9.01	8.85	8.79	8.58	9.23	8.97	8.14	8.80	8.74
O=Cl	–0.02	–0.01	–0.01	–0.01	–0.02	–0.02	–0.02	–0.02	–0.01	0.00	–0.02	–0.02
total	98.53	100.14	107.50	99.05	97.01	99.32	96.37	102.35	98.38	91.10	97.61	95.03
Na	0.031	0.078	0.000	0.000	0.000	0.000	0.000	0.000	0.105	0.000	0.000	0.167
K	0.149	0.128	0.129	0.110	0.151	0.143	0.135	0.146	0.146	0.152	0.215	0.187
Ca	0.721	0.747	0.748	0.701	0.745	0.695	0.710	0.697	0.718	0.729	0.711	0.729
P	0.006	0.000	0.004	0.000	0.013	0.004	0.000	0.015	0.010	0.004	0.000	0.012
Mo	2.074	2.127	2.133	2.047	2.004	2.133	2.102	2.038	2.047	2.097	2.085	1.989
S	0.062	0.065	0.053	0.033	0.078	0.057	0.069	0.066	0.044	0.084	0.046	0.089
U	3.000	3.000	3.000	3.000	3.000	3.000	3.000	3.000	3.000	3.000	3.000	3.000
Cl	0.026	0.023	0.021	0.023	0.027	0.027	0.043	0.033	0.023	0.000	0.031	0.036
OH	3.308	3.292	3.221	3.330	3.409	3.114	3.169	3.253	3.453	3.235	3.343	3.584
H_2O	5	5	5	5	5	5	5	5	5	5	5	5

H_2O* – content calculated on the basis of charge balance and 5 H_2O molecules in the crystal structure.

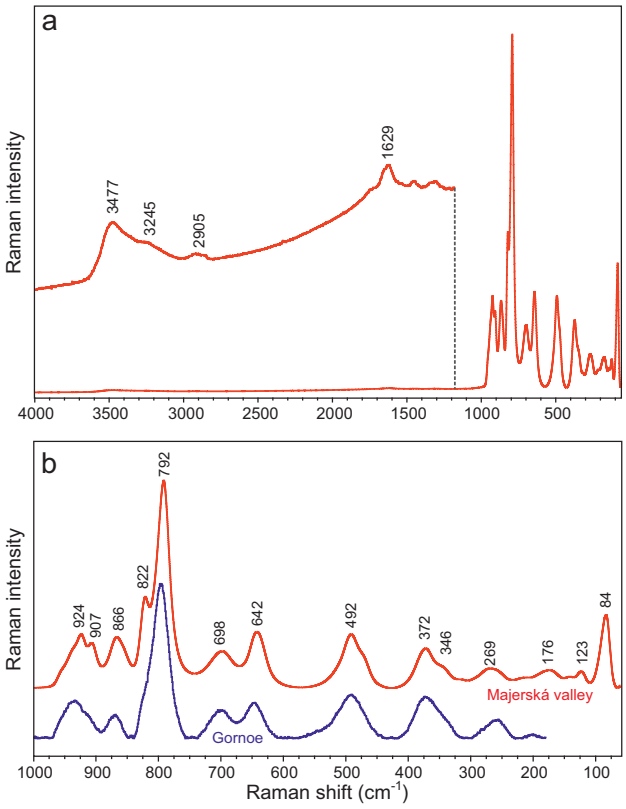

Fig. 4 Raman spectrum of calcurmolite from the Majerská valley: **a** – in the full range; in detail, intensity in the range of the H_2O/OH vibrations increased for clarity; **b** – in the range 1000–60 cm^{-1} with comparison with calcurmolite from the locality Gornoe U deposit, Transbaikal region, Russia (R070028 of the RRUFF database, Lafuente et al. 2015).

(2.85, 2.72 and 2.64 Å) are comparable with data derived from the crystal structure study (Steciuk et al. 2020). A very weak band at 1629 cm^{-1} (Fig. 4a) is attributed to the ν_2 bending vibrations of water molecules. Medium strong and strong bands in the area 1000–750 cm^{-1} are assigned to overlapped stretching vibrations of uranyl groups and Mo octahedra. Most likely medium strong bands at 924 and 907 cm^{-1} are related to antisymmetric stretching vibration ν_3 UO_2^{2+}, with corresponding U–O lengths 1.77 and 1.78 Å, a band at 866 cm^{-1} is connected to symmetric stretching vibration of Mo-O bonds in Mo octahedra and very strong band at 792 cm^{-1} with shoulder at 822 cm^{-1} to symmetric stretching vibration ν_3 UO_2^{2+}, with corresponding U–O lengths 1.82 and 1.79 Å. Medium-intensity bands at 698 and 642 cm^{-1} may be attributed to antisymmetric stretching vibrations of Mo-O bonds in Mo octahedra. A possible coincidence with the libration modes of water molecules, which are usually located in this area (Čejka 1999), cannot be excluded. Bands at 492, 372 cm^{-1} with shoulder 346 cm^{-1} are assigned to the bending vibrations Mo-O bonds in Mo octahedra. A weak band at 269 cm^{-1} is related to the ν_2 UO_2^{2+} bending vibration. Bands at 176, 123 and 84 cm^{-1} may be attributed to the rotational and translational modes as well the lattice vibrational modes.

4.2. Iriginite

It is the second most common uranyl molybdate at the Majerská valley U–Mo occurrence. It occurs as canary to light yellow microcrystalline aggregates and coatings (Fig. 5a), consist of well developed, tabular to columnar crystals up to 12 μm in size (Fig. 5b). Paragenetically, iriginite is the youngest uranyl molybdate at the studied locality.

The experimental powder X-ray pattern of iriginite from the Majerská valley (Tab. 3) agree very well with data calculated from the crystal structure of iriginite (Krivovichev and Burns 2000b). The refined unit-cell parameters (orthorhombic space group *Pbcm*, *a* 6.6871(7), *b* 12.7750(14), *c* 11.5212(12) Å and *V* 984.22(13) $Å^3$) correspond to data published for synthetic iriginite by

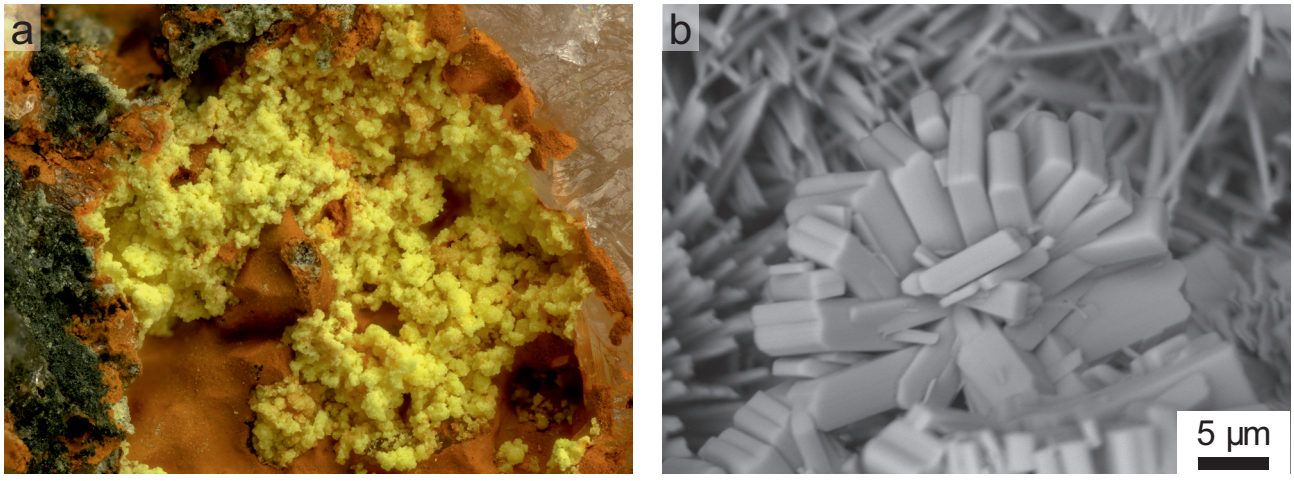

Fig. 5 Iriginite appearance: **a** – Typical light-yellow microcrystalline aggregates of iriginite associated with brown iron oxides. Field of view is 5 mm, photo L. Hrdlovič; **b** – Detail on group of tabular iriginite crystals resting on acicular calcurmolite. BSE photo L. Váchová.

Tab. 3 Powder X-ray diffraction data of iriginite from the Majerská valley occurrence

$d_{obs.}$	$I_{obs.}$	$d_{calc.}$	h	k	l	$d_{obs.}$	$I_{obs.}$	$d_{calc.}$	h	k	l	$d_{obs.}$	$I_{obs.}$	$d_{calc.}$	h	k	l
6.6903	2.1	6.6871	1	0	0	2.564	1.8	2.564	2	3	1	1.763	2.4	1.763	3	0	4
6.3859	100.0	6.3875	0	2	0	2.337	1.5	2.337	1	5	1	1.742	1.6	1.742	3	4	2
5.7626	3.5	5.7606	0	0	2	2.309	1.5	2.309	2	4	0	1.740	0.3	1.740	1	7	1
5.5892	1.1	5.5864	0	2	1	2.157	2.8	2.157	3	1	1	1.733	0.5	1.733	2	3	5
5.2704	10.0	5.2687	1	1	1	2.148	3.6	2.148	1	1	5	1.715	0.3	1.715	2	6	2
4.3653	3.3	4.3645	1	0	2	2.143	2.0	2.144	2	4	2	1.699	2.1	1.699	3	2	4
4.2789	6.2	4.2779	0	2	2	2.126	1.8	2.129	0	6	0	1.665	1.3	1.665	2	0	6
3.6033	3.8	3.6036	1	2	2	2.096	0.6	2.094	0	6	1	1.658	0.7	1.658	1	5	5
3.4296	4.7	3.4291	1	3	1	2.079	3.9	2.079	3	0	2	1.646	0.8	1.646	0	4	6
3.3446	14.5	3.3435	2	0	0	2.065	1.0	2.065	2	2	4	1.641	3.1	1.641	4	1	1
3.2229	42.5	3.2226	1	1	3	2.028	3.5	2.027	1	5	3	1.611	1.1	1.611	2	2	6
3.1953	16.7	3.1938	0	4	0	1.999	1.4	1.999	2	5	1	1.600	1.6	1.600	1	7	3
3.1144	14.7	3.1142	2	1	1	1.977	3.4	1.977	3	2	2	1.542	2.3	1.543	3	4	4
3.0792	2.1	3.0777	0	4	1	1.947	0.7	1.946	3	3	1	1.523	0.5	1.524	2	6	4
2.9627	8.1	2.9623	2	2	0	1.939	1.1	1.939	1	3	5	1.488	0.6	1.487	3	6	2
2.8918	2.9	2.8917	2	0	2	1.920	2.9	1.920	0	0	6	1.476	0.8	1.477	2	4	6
2.7940	1.3	2.7932	0	4	2	1.906	1.0	1.906	3	1	3	1.467	1.2	1.467	2	1	7
2.6454	1.4	2.6453	1	0	4	1.877	1.3	1.877	2	1	5	1.430	0.3	1.429	3	6	3
2.6335	3.1	2.6344	2	2	2	1.839	3.7	1.839	0	2	6	1.426	0.6	1.426	0	6	6
2.6238	6.7	2.6233	1	3	3	1.796	1.2	1.796	2	6	0						

Krivovichev and Burns (2000b): a 6.705(1), b 12.731(2), c 11.524(2) Å and V 983.6(2) Å^3.

Quantitative WDS chemical analyses of iriginite from the Majerská valley occurrence and the corresponding empirical formulae are shown in Tab. 4. There is only a limited amount of compositional data of natural iriginite available in the literature; older works (e.g., Soboleva and Pudovkina 1957; Epshtein 1959; Stephenson 1964) reported the presence of minor amounts of Ca or Fe, except for U and Mo. Recently, Pauliš et al. (2019) observed

Tab. 4 Quantitative chemical analyses of iriginite from the Majerská valley occurrence (in wt. %) and the calculated empirical formulae (*apfu*).

	mean	1	2	3	4	5	6	7	8	9	10	11
K_2O	0.10	0.13	0.16	0.14	0.13	0.08	0.10	0.05	0.09	0.07	0.08	0.11
CaO	0.01	0.00	0.00	0.00	0.00	0.00	0.00	0.00	0.00	0.00	0.07	0.00
FeO	2.85	2.74	2.78	2.38	2.47	2.98	2.77	3.92	2.82	2.78	2.71	2.96
SiO_2	0.07	0.25	0.27	0.28	0.00	0.00	0.00	0.00	0.00	0.00	0.00	0.00
As_2O_5	0.02	0.00	0.00	0.00	0.00	0.00	0.26	0.00	0.00	0.00	0.00	0.00
P_2O_5	0.08	0.00	0.14	0.07	0.12	0.03	0.12	0.07	0.13	0.14	0.03	0.02
MoO_3	43.10	43.46	44.93	42.92	42.08	43.54	43.81	42.12	43.73	39.95	43.50	44.08
SO_3	0.63	0.53	0.67	0.86	0.44	0.73	0.62	0.75	0.61	0.55	0.51	0.66
UO_3	46.44	46.12	47.29	46.19	46.24	47.36	47.61	44.79	47.86	44.28	45.81	47.25
Cl	0.10	0.11	0.10	0.08	0.13	0.11	0.07	0.11	0.09	0.11	0.09	0.09
H_2O*	8.77	8.71	8.94	8.73	8.74	8.95	9.00	8.46	9.04	8.37	8.66	8.93
O=Cl	–0.02	–0.02	–0.02	–0.02	–0.03	–0.02	–0.02	–0.02	–0.02	–0.02	–0.02	–0.02
total	102.15	102.03	105.25	101.63	100.32	103.75	104.34	100.25	104.35	96.22	101.44	104.08
K	0.014	0.017	0.021	0.018	0.017	0.010	0.013	0.007	0.011	0.010	0.011	0.014
Ca	0.001	0.000	0.000	0.000	0.000	0.000	0.000	0.000	0.000	0.000	0.008	0.000
Fe	0.244	0.237	0.234	0.205	0.213	0.251	0.232	0.348	0.235	0.250	0.236	0.249
Si	0.007	0.026	0.027	0.029	0.000	0.000	0.000	0.000	0.000	0.000	0.000	0.000
As	0.001	0.000	0.000	0.000	0.000	0.000	0.014	0.000	0.000	0.000	0.000	0.000
P	0.007	0.000	0.012	0.006	0.010	0.003	0.010	0.006	0.011	0.013	0.003	0.002
Mo	1.844	1.873	1.888	1.846	1.808	1.827	1.829	1.869	1.816	1.793	1.887	1.854
S	0.048	0.041	0.051	0.067	0.034	0.055	0.047	0.060	0.046	0.044	0.040	0.050
U	1.000	1.000	1.000	1.000	1.000	1.000	1.000	1.000	1.000	1.000	1.000	1.000
Cl	0.017	0.019	0.017	0.014	0.023	0.019	0.012	0.020	0.015	0.020	0.016	0.015
O*	6.701	6.760	6.777	6.613	6.585	6.668	6.636	6.879	6.618	6.560	6.858	6.758
H_2O	3	3	3	3	3	3	3	3	3	3	3	3

H_2O* – content calculated on the basis of 3 H_2O molecules in the crystal structure; O* – calculated on the basis of charge balance

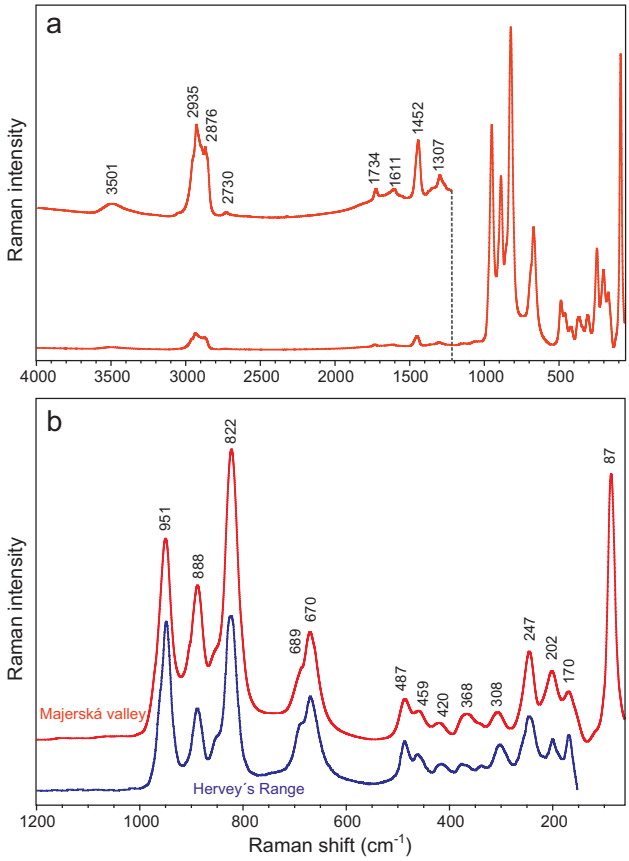

Fig. 6 Raman spectrum of iriginite from the Majerská valley: **a** – in the full range; in detail, intensity in the range of the H_2O vibrations increased for clarity; **b** – in the range 1200–60 cm^{-1} with comparison with iriginite from the Hervey´s Range deposit, Australia (R060269 of the RRUFF database, Lafuente et al. 2015).

elevated Fe concentrations (up to 0.14 *apfu*) and minor Cu in iriginite from Vrchoslav, Czech Republic. Studied iriginite shows elevated contents of Fe (up to 0.35 *apfu*) and S (up to 0.07 *apfu*) as well as minor amounts of Si (up to 0.03 *apfu*), K and Cl (both up to 0.02 *apfu*) or Ca, P and As (up to 0.01 *apfu*). The average ($n = 11$) empirical formula of iriginite form the Majerská valley occurrence, calculated on the basis of basis of U = 1 *apfu* is $(Fe_{0.24}K_{0.01})_{\Sigma 0.25}(UO_2)Mo_{1.84}O_{6.70}Cl_{0.02}(SO_4)_{0.05}(PO_4)_{0.01}(SiO_4)_{0.01}\cdot 3H_2O$.

The full-range Raman spectrum of the iriginite from the Majerská valley occurrence is given in Fig. 6a; it agrees very well with the spectrum of iriginite from the Hervey´s Range deposit, Australia (Fig. 6b) (R060269 of the RRUFF database, Lafuente et al. 2015) and is similar to published spectra of iriginite from Hervey´s Range deposit, Australia (Frost et al. 2004) or Vrchoslav, Czech Republic (Pauliš et al. 2019). Weak bands at 3501, 2935, 2876, and 2730 cm^{-1} (Fig. 6a) are assigned to the O–H stretching vibration of hydrogen bonded water molecules. Calculated O–H···O hydrogen-bond lengths (2.90, 2.65, 2.63 and 2.60 Å) are comparable with data from the structural study of iriginite (Krivovichev and Burns 2000b). A band of the very low intensity, located at 1611 cm^{-1} is attributed to the ν_2 bending vibrations of water molecules. Very weak and broad bands at 1734, 1452 and 1307 cm^{-1} (Fig. 6a) may be associated with overtones and combination modes. Very strong bands at 951 and 822 cm^{-1} (Fig. 6b) are assigned to the ν_3 UO_2^{2+} antisymmetric and ν_1 UO_2^{2+} symmetric stretching vibrations, respectively, corresponding U–O bond lengths in uranyl (1.75 and 1.79 Å) are comparable with data derived from the X-ray studies for iriginite (1.77–1.79 Å, Krivovichev and Burns 2000b). Strong band at 888 cm^{-1} is probably related to the symmetric stretching vibration of Mo–O bonds in Mo octahedra. A band at 670 cm^{-1} with a shoulder at 689 cm^{-1} is attributed to the antisymmetric stretching vibrations of Mo–O bonds in Mo octahedra, a possible coincidence with the libration modes of water molecules (Čejka 1999) cannot be excluded. A series of

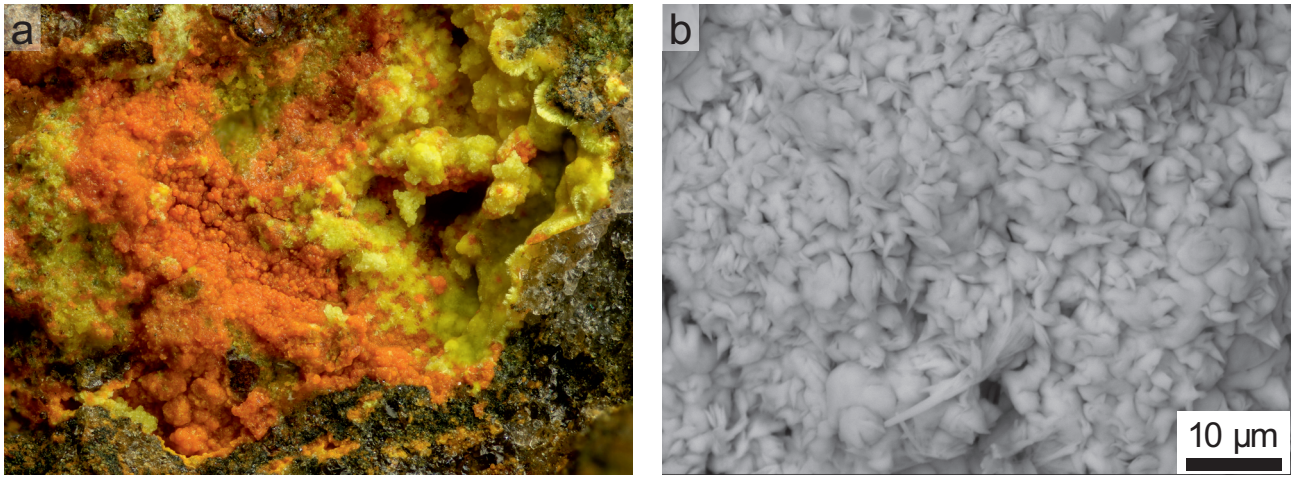

Fig. 7 Appearance of umohoite associated with calcurmolite: **a** – Red-orange microcrystalline coatings and aggregates of umohoite closely associated with bright yellow acicular calcurmolite. Field of view is 5 mm, photo L. Hrdlovič; **b** – Detail on group of poorly developed and curved platy crystals of umohoite with one elongated acicular crystal of calcurmolite resting on umohoite. BSE photo L. Váchová.

bands at 487, 459, 420, 368 and 308 cm^{-1} are assigned to bending vibrations Mo–O bonds in Mo octahedra. Bands at 247 and 202 cm^{-1} are related to the ν_2 UO_2^{2+} doubly degenerate bending vibrations. Bands at 170 and 87 cm^{-1} may be attributed to the rotational and translational modes and the lattice vibrational modes.

4.3. Umohoite

Umohoite is a rare mineral at the studied locality. It forms red-orange to bright orange microcrystalline aggregates and coatings (Fig. 7a) consisting of poorly developed, curved platy crystals up to 5 μm in size (Fig. 7b). Umohoite is mostly slightly younger than calcurmolite and older than iriginite.

Powder X-ray data of umohoite were not obtained due to the very small amount of pure material available. Quantitative WDS chemical analyses of umohoite from the Majerská valley occurrence and the corresponding empirical formulae are shown in Tab. 5. Published compositional data of umohoite from various worldwide occurrences (e.g., Brophy and Kerr 1953; Skvortsova et al. 1961; Deliens 1975; Piret and Deliens 1976, 1977; Belova et al. 1985; Sidorenko et al. 2003; Dal Bo et al. 2018) indicate the frequent presence of numerous other elements in addition to U and Mo, especially Na, Ca, Fe, Ni, Cu, P, As or Si. This is caused by the versatile topology of umohoite crystal structure and the presence of two symmetrically distinct interlayers, which allows accommodation of other cations (Krivovichev and Burns 2000a). Umohoite from the Majerská valley occurrence contains significant amounts of Fe (up to 0.36 *apfu*), K (up to 0.16 *apfu*) and Ca (up to 0.19 *apfu*) as well as minor concentrations of Mg (up to 0.04 *apfu*), S (up to 0.03 *apfu*), and locally also Al, P, and Cl (all up to 0.01 *apfu*). The average (n = 6) empirical formula of studied umohoite calculated on the basis of U = 1 *apfu* is $(Fe_{0.29}Ca_{0.14}K_{0.08}Mg_{0.02}Al_{0.01})_{\Sigma 0.54}(UO_2)(MoO_4)_{1.00}(SO_4)_{0.02}\cdot 2H_2O$.

Tab. 5 Quantitative chemical analyses of umohoite from the Majerská valley occurrence (in wt. %) and the calculated empirical formulae (*apfu*).

	mean	1	2	3	4	5	6
K_2O	0.77	0.55	0.61	0.61	0.46	0.86	1.52
CaO	1.62	1.84	1.73	1.63	2.15	1.13	1.25
FeO	4.21	4.07	4.18	3.91	4.58	5.24	3.27
MgO	0.17	0.18	0.11	0.19	0.15	0.31	0.08
Al_2O_3	0.09	0.00	0.00	0.13	0.14	0.13	0.13
SiO_2	0.06	0.00	0.00	0.00	0.00	0.00	0.34
P_2O_5	0.04	0.03	0.01	0.02	0.01	0.05	0.11
MoO_3	29.48	29.52	29.83	29.29	29.28	29.80	29.15
SO_3	0.30	0.29	0.33	0.45	0.17	0.30	0.25
UO_3	58.44	59.65	58.65	58.71	56.54	58.53	58.54
Cl	0.03	0.07	0.00	0.00	0.06	0.00	0.07
H_2O*	7.36	7.51	7.39	7.40	7.12	7.37	7.37
O=Cl	–0.01	–0.02	0.00	0.00	–0.01	0.00	–0.02
total	102.55	103.70	102.84	102.34	100.65	103.72	102.07
K	0.080	0.056	0.063	0.063	0.049	0.089	0.158
Ca	0.142	0.157	0.150	0.142	0.194	0.098	0.109
Fe	0.287	0.272	0.284	0.265	0.322	0.356	0.222
Mg	0.021	0.021	0.013	0.023	0.019	0.038	0.010
Al	0.008	0.000	0.000	0.012	0.014	0.012	0.012
Si	0.005	0.000	0.000	0.000	0.000	0.000	0.028
P	0.003	0.002	0.001	0.001	0.001	0.003	0.008
Mo	1.002	0.983	1.011	0.991	1.029	1.012	0.990
SO	0.018	0.017	0.020	0.027	0.011	0.018	0.015
U	1.000	1.000	1.000	1.000	1.000	1.000	1.000
Cl	0.005	0.009	0.000	0.000	0.009	0.000	0.010
H_2O	2	2	2	2	2	2	2

H_2O* – content calculated on the basis of 2 H_2O molecules in the crystal structure.

The full-range Raman spectrum of the studied umohoite is provided in Fig. 8a; it is only partly similar to the spectrum of green umohoite from the Kyzylsai deposit, Kazakhstan, with relatively low quality (Fig. 8b) (R061135 of the RRUFF database, Lafuente et al. 2015). A weak and broad band at 3487 cm^{-1} (Fig. 8a) is attributed to the ν O-H stretching vibration of hydrogen-bonded water molecules. The calculated O–H···O hydrogen-bond length (2.85 Å) is comparable with data determined during the crystal structure study of umohoite (Krivovichev and Burns 2000a). A weak band at 1632 cm^{-1} (Fig. 8a) is assigned to the ν_2 bending vibrations of water molecules. Medium strong band at 969 cm^{-1} is probably related to the ν_3 UO_2^{2+} antisymmetric stretching vibration and very strong bands at 844 and 795 cm^{-1} to the ν_1 UO_2^{2+} symmetric stretching vibrations; corresponding U–O bond lengths in uranyl (1.74, 1.77 and 1.82 Å) are comparable with data derived from the X-ray studies for umohoite (1.77–1.80 Å, Krivovichev and Burns 2000a). Strong bands at 899 and 709 cm^{-1} are probably connected to symmetric and antisymmetric stretching vibrations of the Mo–O bonds in Mo octahedra. In the case of the band at 709 cm^{-1} is not possible to exclude a coincidence with the libration modes of water. Bands at 475 and 377 cm^{-1} are attributed to the bending vibrations Mo–O bonds in Mo octahedra. Bands at 291 and 246 cm^{-1} are related to the ν_2 UO_2^{2+} bending vibration. Bands below 200 cm^{-1} (148, 106 and 73 cm^{-1}) may be assigned to rotational and translational modes as well as the lattice vibrational modes.

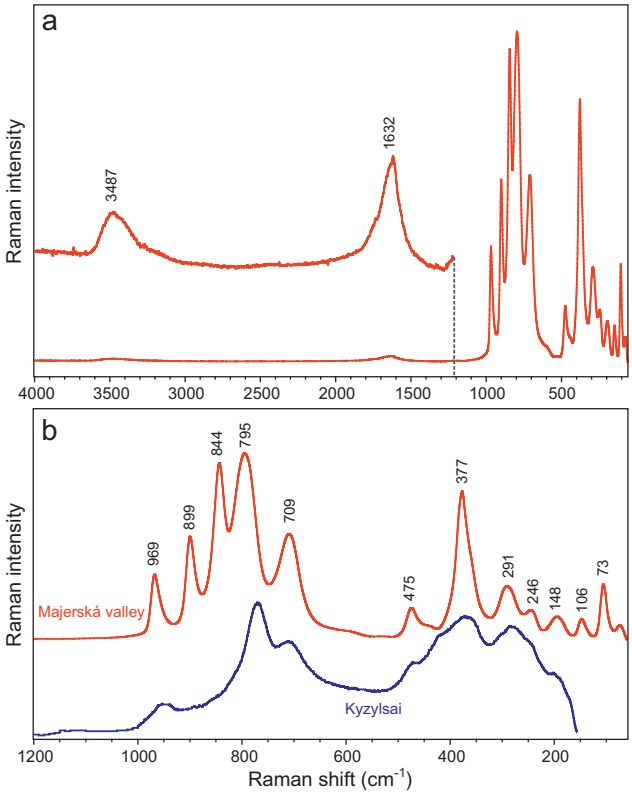

Fig. 8 Raman spectrum of umohoite from the Majerská valley: **a** – in the full range; in detail, intensity in the range of the H_2O vibrations increased for clarity; **b** – in the range 1200–60 cm^{-1} with comparison with umohoite from the Kyzylsai deposit, Kazakhstan (R061135 of the RRUFF database, Lafuente et al. 2015).

5. Conclusions

A new occurrence of three rare uranyl molybdates, calcurmolite, iriginite and umohoite was recently discovered at the Majerská valley U–Mo prospect near Čučma, Slovakia. Detailed paragenetic, compositional and Raman spectroscopic features of all three minerals are discussed in this paper. The studied assemblage of uranyl molybdates represents *in-situ* weathering products of supergene alteration of uraninite–molybdenite aggregates under the acidic conditions, which were induced by the weathering of abundant pyrite. Calcium, which is an essential element in calcurmolite, was most probably provided by the breakdown of accessory fluorapatite. Other supergene uranyl minerals, such as phosphorus-dominant members of the autunite group (autunite, bassetite, saléeite, and torbernite) were formed in the distant areas of the quartz vein, where conditions/pH of supergene solutions were slightly less acidic to neutral.

Acknowledgements. We would like to thank the handling editor Jakub Plášil, for his helpful comments. We are also thankful for the reviews of Anatoly Kasatkin and Evgeny Nazarchuk and for their comments which helped us to improve the manuscript as well as to Luboš Hrdlovič, Lenka Váchová and Pavol Myšľan for the technical support of this research. This study was financially supported by the Slovak Research and Development Agency (contract No. APVV-22-0041), Research Agency of the Ministry of Education, Science, Research and Sport of the Slovak Republic (contracts No. VEGA 1/0574/25). and by the Ministry of Culture of the Czech Republic (long-term project DKRVO 2024-2028/1.II.b; National Museum, 00023272) as well as EU NextGenerationEU through the Recovery and Resilience Plan for Slovakia under the project No. 09I03-03-V06-00107.

References

Alekseev EV, Krivovichev SV, Malcherek T, Depmeier W (2007) One-dimensional array of two- and three-center cation–cation bonds in the structure of $Li_4[(UO_2)_{10}O_{10}(Mo_2O_8)]$. Inorg Chem 46: 8442–8444

Bajaník Š, Ivanička J, Mello J, Pristaš J, Reichwalder P, Snopko L, Vozár J, Vozárová A (1984) Geological map of the Slovenské Rudohorie Mts. – eastern part 1 : 50 000. Dionýz Štúr Institute of Geology, Bratislava

Bartlett JR, Cooney RP (1989) On the determination of uranium-oxygen bond lengths in dioxouranium (VI) compounds by Raman spectroscopy. J Mol Struct 193: 295–300

Belova LN, Fedorov OV, Lyubomilova GV, Vishnev AI (1985): Ferriferrous umohoite. Izv Akad Nauk SSSR Ser Geol 1985(12): 131–135

Brophy GP, Kerr PF (1953) Hydrous uranium molybdate in Marysvale ore. Annual Report for June 30, 1952 to April 1, 1953, U.S. Atomic Energy Comm RME-3046: 45–51

Buck EC, Wronkiewicz DJ, Finn PA, Bates JK (1997) A new uranyl oxide hydrate phase derived from spent fuel alteration. J Nucl Mater 249: 70–76.

Burnham CW (1962) Lattice constant refinement. Carnegie Institute Washington Yearbook 61: 132–135

Burns PC (1999): The crystal chemistry of uranium. In: Burns PC, Ewing RC (eds) Uranium: Mineralogy, Geochemistry and the Environment. Rev Mineral Geochem 38: pp 23–90

Čejka J (1999) Infrared spectroscopy and thermal analysis of the uranyl minerals. Rev Mineral 38: 521–622

Chen Z, Luo K, Tan F, Zhang Y, Gu X (1986) Tengchongite, a new mineral of hydrated calcium uranyl molybdate. Kexue Tongbao 31(6): 396–401

Chen Z, Huang Y, Gu X (1990) A new uranium mineral – Yingjiangite. Acta Mineral Sin 10: 102–105

Chernikov AA, Pekov IV, Minina EL (1997) On the history of study of uranium minerals in Russia and the USSR. Zap Vses Mineral Obshchst 126: 111–128 (in Russian)

Coleman RG, Appleman DE (1957) Umohoite from the Lucky MC mine, Wyoming. Am Mineral 42: 657–660

Dal Bo F, Hatert F, Philippo S (2018) Supergene Uranyl Mineralization of the Rabejac Deposit, Lodève, France. Minerals 8: 414

Deliens M (1975) Une association de molybdates d'uranium de Shinkolobwe (région du Shaba, République du Zaïre). Ann Soc Géol Belgique 98: 155–160

Deliens M (1992) Etude comparative des calcurmolites de Rabejac (Lodève, Herault, France) et de l'Union Sovietique. Ann Soc Geol Belg 115: 91–97

Donát A (1998) Ocenenie výskytov anomálií prvkov vzácnych zemín v perme a gelnickej skupine SGR, Záverečná správa. MS, ŠGÚDŠ-Geofond (83224), 1–319

Elliot P, Plášil J, Petříček V, Čejka J, Bindi L (2019) Twinning and incommensurate modulation in baumoite, $Ba_{0.5}[(UO_2)_3O_8Mo_2(OH)_3](H_2O)_{\sim 3}$, the first natural Ba uranyl molybdate. Mineral Mag 83: 507–514

Epshtein GY (1959) On uranyl molybdates – moluranite and iriginite. Zap Vses Mineral Obshchst 88: 564–569 (in Russian)

Fedorov OV (1963) The second finding of the calcium molybdate of uranium in the USSR. Zap Vses Mineral Obshchst 92: 464–465 (in Russian)

Ferenc Š, Mikuš T, Spišiak J, Milovská S (2019) Supergene minerals in quartz±fluorapatite hydrothermal veins with U-Mo and U-REE mineralization near Čučma (Gemeric Unit, Western Carpathians, eastern Slovakia): preliminary study. Abstract, Mineralogicko-petrologická konferencia Petros 2019: 17–19

Ferenc Š, Števko M, Mikuš T, Milovská S, Kopáčik R, Hoppanová E (2021) Primary Minerals and Age of The Hydrothermal Quartz Veins Containing U–Mo–(Pb, Bi, Te) Mineralization in the Majerská Valley near Čučma (Gemeric Unit, Spišsko-Gemerské Rudohorie Mts., Slovak Republic) Minerals 11(6): 629

Finch RJ, Murakami T (1999) Systematics and paragenesis of uranium minerals. In: Burns PC, Ewing RC (eds) Uranium: Mineralogy, Geochemistry and the Environment. Rev Mineral Geochem 38: 91–179

Frost RL, Duong L, Weier M (2004) Raman microscopy of the molybdate minerals koechlinite, iriginite and lindgrenite. N Jb Mineral, Abh 180(3): 245–260

Frost RL, Čejka J, Dickfos MJ (2008) Raman and infrared spectroscopic study of the molybdate-containing uranyl mineral calcurmolite. J Raman Spectrosc 39(7): 779–785

Gröbner J, Kolitsch U (2007) Seltene Mineralien aus dem Uranschurf Tirpersdorf im Sächsischen Vogtland. Lapis 32: 37–58

Hamilton P, Kerr PF (1959) Umohoite from Cameron, Arizona. Am Mineral 44: 1248–1260

Kopchenova EV, Skvortsova KV, Silant'eva NI, Sidorenko GA, Mikhailova LV (1962) Mourite, a new supergene uranium-molybdenum mineral. Zap Vses Mineral Obshchst 91: 67–71 (in Russian)

Kraus W, Nolze G (1996) POWDER CELL – a program for the representation and manipulation of crystal structures and calculation of the resulting X–ray powder patterns. J Appl Crystallogr 29: 301–303

Krivovichev SV, Burns PC (2000a) Crystal chemistry of uranyl molybdates. I. The structure and formula of umohoite. Canad Mineral 38: 717–726

Krivovichev SV, Burns PC (2000b) Crystal chemistry of uranyl molybdates. II. The structure and formula of iriginite. Canad Mineral 38: 847–851

Krivovichev SV, Burns PC (2001a) Crystal chemistry of uranyl molybdates. III. New structural themes in the structures of $Na_6[(UO_2)_2O(MoO_4)_4]$, $Na_6[(UO_2)(MoO_4)_4]$ and $K_6[(UO_2)_2O(MoO_4)_4]$. Canad Mineral 39: 197–206

Krivovichev SV, Burns PC (2001b) Crystal chemistry of uranyl molybdates. IV. Crystal structures of $M2[(UO_2)_6(MoO_4)_7(H_2O)_2]$, M = Cs, NH_4. Canad Mineral 39: 207–214

Krivovichev SV, Burns PC (2002a) Crystal chemistry of rubidium uranyl molybdates: crystal structures of $Rb_6(UO_2)(MoO_4)_4$, $Rb_6(UO_2)_2O(MoO_4)_4$, $Rb_2(UO_2)(MoO_4)_2$, $Rb_2(UO_2)_2(MoO_4)_3$ and $Rb_2(UO_2)_6(MoO_4)_7(H_2O)_2$. J Solid State Chem 168: 245–258

Krivovichev SV, Burns PC (2002b) Crystal chemistry of uranyl molybdates. VI. New uranyl molybdate units in structures of $Cs_4[(UO_2)_3Mo_3O_{14}]$ and $Cs_6[(UO_2)(MoO_4)_4]$. Canad Mineral 40: 201–209

Krivovichev SV, Burns PC (2002c) Crystal chemistry of uranyl molybdates. VII. Iriginite-type polyhedral sheet in the structure of $(UO_2)Mo_2O_7(H_2O)_2$. Canad Mineral 40: 1571–1577

Krivovichev SV, Burns PC (2002d) Synthesis and crystal structure of $Ag_6[(UO_2)_3O(MoO_4)_5]$: a novel sheet of triuranyl clusters and MoO_4 tetrahedra. Inorg Chem 41: 4108–4110

Krivovichev SV, Burns PC (2003a) Crystal chemistry of uranyl molybdates. VIII. Crystal structures of $Na_3Tl_3[(UO_2)(MoO_4)_4]$, $Na_{13-x}Tl_{3+x}[(UO_2)(MoO_4)_3]_4(H_2O)_{6+x}$ (x = 0.1), $Na_3Tl_5[(UO_2)(MoO_4)_3]_2(H_2O)_3$ and $Na_2[(UO_2)(MoO_4)_2](H_2O)_4$. Canad Mineral 41: 707–719

Krivovichev SV, Burns PC (2003b) Synthesis and crystal structure of $Li_2[(UO_2)(MoO_4)_2]$, a uranyl molybdate with chains of corner-sharing uranyl square bipyramids and MoO_4 tetrahedra. Solid State Sci 5: 481–485

Krivovichev SV, Plášil J (2013) Mineralogy and crystallography of uranium. In: Burns PC, Sigmon GE (eds) Uranium: From Cradle to Grave. Mineralogical Association of Canada Short Courses 43: pp 15–119

Kuporev IV, Kalashnikova SA, Gurzhiy VV (2024) Crystal Chemistry and Structural Complexity of the Uranyl Molybdate Minerals and Synthetic Compounds. Crystals 14: 15

Lafuente B, Downs RT, Yang H, Stone N (2015) The power of databases: the RRUFF project. In: Armbruster T, Danisi RM (eds) Highlights in Mineralogical Crystallography, Berlin, Germany, W. De Gruyter: 1–30

Libowitzky E (1999) Correlation of O–H stretching frequencies and O–H···O hydrogen bond lengths in minerals. Monatsh Chem 130: 1047–1059

Lunk HJ, Hartl H, Hartl MA, Fait MJ, Shenderovich IG, Feist M, Frisk TA, Daemen LL, Mauder D, Eckelt R, Gurinov AA (2010) "Hexagonal molybdenum trioxide" – known for 100 years and still a fount of new discoveries. Inorg Chem 49: 9400–9408

Moura JVB, Silveira JV, da Silva Filho JG, Souza Filho AG, Luz-Lima C, Freire PTC (2018) Temperature-induced phase transition in h-MoO_3: Stability loss mechanism uncovered by Raman spectroscopy and DFT calculations. Vibrat Spectrosc 98: 98–104

Nakamoto K (2009) Infrared and Raman spectra of inorganic and coordination compounds Part A: Theory and applications in inorganic chemistry. John Wiley and Sons Inc. Hoboken, New Jersey

Nazarchuk EV, Krivovichev SV, Burns PC (2005a) Crystal structure and phase transformations of $Ca[(UO_2)_6(MoO_4)_7(H_2O)_2](H_2O)_n$ (n~7.6). Zap Ross Mineral 134: 110–117

Nazarchuk EV, Krivovichev SV, Burns PC (2005b) Crystal structure of $Tl_2[(UO_2)_2(MoO_4)_3]$ and crystal chemistry of the compounds $M_2[(UO_2)_2(MoO_4)_3]$ (M = Tl, Rb, Cs). Radiochemistry 47: 408–411

Nazarchuk EV, Tagirova YG, Charkin DO, Krzhizhanovskaya MG, Kasatkin AV, Krivovichev SV, Gurzhiy VV (2025) Crystal structure and high-temperature behavior of synthetic mourite, $(UO_2)Mo_5O_{14}(OH)_4(H_2O)_2$. Russ Geol Geophys 66: 732–742

Obbade S, Yagoubi S, Dion C, Saadi M, Abraham F (2003) Synthesis, crystal structure and electrical characterization of two new potassium uranyl molybdates $K_2(UO_2)_2(MoO_4)O_2$ and $K_8(UO_2)_8(MoO_5)_3O_6$. J Solid State Chem 174: 19–31

Ondruš P (1993) A computer program for analysis of X-ray powder diffraction patterns. Materials Science Forum, EPDIC-2, Enchede, 133–136, 297–300

Pauliš P, Vrtiška L, Fuchs P, Adamovič J, Čejka J, Pour O, Malíková R (2019) Iriginit, chistyakovait a metazeunerit ze štoly 5. květen ve Vrchoslavi v Krušných horách (Česká republika). Bull Mineral Petrolog Odd Nár Muz (Praha) 27(1): 136–147 (in Czech)

Piret P, Deliens M (1976) Nouvelles données sur une umohoite magnésienne de Shinkolobwe (région du Shaba, Zaïre). Ann Soc Géol Belgique 99: 205–209

Piret P, Deliens M (1977) Description de deux variétés nickelifères d'umohoïte de Shinkolobwe (région du Shaba, Zaïre). Ann Soc Géol Belgique 100: 41–45

Pouchou JL, Pichoir F (1985) "PAP" (φρZ) procedure for improved quantitative microanalysis. In: Armstrong JT (ed) Microbeam Analysis. San Francisco Press, San Francisco, pp 104–106

Robinson GW, Carlson SM (2013) Mineralogy of Michigan Update. A.E. Seaman Mineral Museum, Michigan Technological University, Houghton, Michigan. 1–46

Rudnitskaya LS (1959) Calcium molybdate of uranium. Yadernoe Gor I Reakt Met 3: 160–161

Sarp H, Chiappero PJ (1992) Deloryite, $Cu_4(UO_2)(MoO_4)_2(OH)_6$ a new mineral from Cap Garonne mine near Le Pradet, Var, France. N Jb Mineral Mh 2: 58–64

Sidorenko GA, Rastsvetaeva RK, Chukanov NV, Chistyakova NI, Barinova AV (2003) Umohoite: new data on its mineralogy and crystal-chemistry. Zap Vser Mineral Obshchest 132(3): 73–80 (in Russian)

Sidorenko GA, Chistyakova NI, Chukanov NV, Naumova IS, Rassulov VA (2005) Calcurmolite: new data on chemical composition and constitution of the mineral. New Dat Min M 40: 29–36

Skvortsova KV, Sidorenko GA (1965) Sedovite, a new supergene mineral of uranium and molybdenum. Zap Vses Mineral Obshchst 94(5): 548–554

Skvortsova KV, Kopchenova EV, Silant'eva NI, Sidorenko GA, Dara AD (1961) On the conditions of umohoite formation on U.S.S.R. uranium–molybdenum deposits. Geology of Ore Deposits 5: 53–63 (in Russian)

Skvortsova KV, Kopchenova EV, Sidorenko GA, Kuznetsova NN, Dara AD, Rybakova LI (1969) Calcium–sodium uranomolybdates. Zap Vses Mineral Obshchst 98: 679–688 (in Russian)

Soboleva MV, Pudovkina IA (1957) Uranium Minerals: Handbook. Gosgeoltekhizdat, Moscow, pp 1–409

Steciuk G, Škoda R, Rohlíček J, Plášil J (2020) Crystal structure of the uranyl–molybdate mineral calcurmolite $Ca[(UO_2)_3(MoO_4)_2(OH)_4](H_2O)_{\sim 5.0}$: insights from a precession electron-diffraction tomography study. J Geosci 65: 15–25

Stephenson DA (1964) Iriginite from South Dakota. Am Min (49): 408–414

Števko M (2022) Prehľad nových nálezov z vybraných lokalít v Spišsko-gemerskom rudohorí. Minerál 30 (5): 387–413 (in Slovak)

Šváb E, Tulis J, Badár J (1966) Záverečná správa o výsledkoch geologicko-prieskumných prác locality Čučma. MS, ŠGÚDŠ-Geofond (34_T), 1–113 (in Slovak)

Vargas-Consuelos CI, Camacho-López MA, Ramos-Sanchez VH, Graeve OA (2023) Phase and morphology control of hexagonal MoO_3 crystals via Na^+ interactions: a Raman spectroscopy study. J Phys Chem C 127(27): 13136–13148